Activating mutation in a mucolipin transient receptor potential channel leads to melanocyte loss in varitint–waddler mice

Haoxing Xu*†, Markus Delling*, Linyu Li*, Xianping Dong*†, and David E. Clapham*‡

*Department of Cardiology, Howard Hughes Medical Institute, Children's Hospital Boston and Department of Neurobiology, Harvard Medical School, Enders Building 1309, 320 Longwood Avenue, Boston, MA 02115

Contributed by David E. Clapham, September 27, 2007 (sent for review September 22, 2007)

Transient receptor potential (TRP) genes of the mucolipin subfamily (TRPML1–3 and MCOLN1–3) are presumed to encode ion channel proteins of intracellular endosomes and lysosomes. Mutations in human *TRPML1* (mucolipin 1/MCOLN1) result in mucolipidosis type IV, a severe inherited neurodegenerative disease associated with defective lysosomal biogenesis and trafficking. A mutation in mouse TRPML3 (A419P; TRPML3^{Va}) results in the varitint–waddler (*Va*) phenotype. *Va* mice are deaf, exhibit circling behavior due to vestibular defects, and have variegated/dilute coat color as a result of pigmentation defects. Prior electrophysiological studies of presumed TRPML plasma membrane channels are contradictory and inconsistent with known TRP channel properties. Here, we report that the *Va* mutation produces a gain-of-function that allows TRPML1 and TRPML3 to be measured and identified as inwardly rectifying, proton-impermeant, Ca^{2+}-permeant cation channels. TRPML3 is highly expressed in normal melanocytes. Melanocyte markers are lost in the *Va* mouse, suggesting that their variegated and hypopigmented fur is caused by severe alteration of melanocyte function or cell death. TRPML3^{Va} expression in melanocyte cell lines results in high resting Ca^{2+} levels, rounded, poorly adherent cells, and loss of membrane integrity. We conclude that the *Va* phenotype is caused by mutation-induced TRPML3 gain-of-function, resulting in cell death.

calcium channel | lysosome | mucolipidosis | TRPML | hair

TRPML1 is a putative intracellular ion channel that colocalizes with late endosomal/lysosomal markers (1–3). TRPML2 and TRPML3 are less well understood but are also presumed to be primarily intracellular channels that mediate ion fluxes across endosomal membranes (4). TRPML3 is mutated in varitint–waddler (*Va* and *VaJ*) mice (5). Mice homozygous or heterozygous for the *Va* (A419P) mutation are deaf and exhibit circling behavior indicative of a vestibular defect. Heterozygotes display a variegated and dilute coat color, whereas homozygotes are almost white and have reduced viability (6). A second mutation in TRPML3 arising in the original *Va* stock (A419P; I362T) results in a less-severe (*VaJ*) phenotype (7).

Mucolipin channel function is unclear because of conflicting data from heterologously expressed, presumed TRPML currents. TRPML1 was claimed to underlie nonselective outwardly rectifying monovalent (8) or proton-conducting (9) currents, but neither of these results were reproduced by others (1). Here, we show that the A419P mutation in the presumed segment (S)4–S5 linker results in a constitutively active, inwardly rectifying cation channel that can be measured across the cell's plasma membrane. Mutation of the corresponding amino acids in TRPML1 results in similar overall conductance properties. WT TRPML3 is highly expressed in melanocytes, but these cells are lost in *Va*/*Va* mice, as assessed by the disappearance of melanocyte markers. Consistent with the toxicity of TRPML3^{Va} expression in melanocyte cell lines, we hypothesize that the loss of fur color is caused by the loss of functioning melanocytes.

Results

TRPML3 mRNA is abundant in the cochlea (particularly the stria vascularis) (Fig. 1 *A* and *B*) and hair follicles of postnatal day (P)0 mice (Fig. 1*C*). In hair follicles, we observed prominent staining in a subset of cells along the hair shaft and in the hair bulb (Fig. 1 *C* and *D*). The distribution of TRPML3 at P0 is similar to the distribution of melanocytes that later migrate to the bottom of the hair follicle and localize to the hair bulb (10). We generated antibodies that were specific to TRPML3, as shown by immunohistochemistry and Western blotting [supporting information (SI) Fig. 6]. Both homozygous (Fig. 1*E*) and heterozygous *Va* mice exhibit a fur color defect. TRPML3-specific immunolabeling of skin sections from P4 WT mice showed specific cytoplasmic staining of cells in the hair follicles, particularly in cells of the upper region of the hair bulb (Fig. 1*F*), consistent with the location of mature melanocytes at this developmental stage (11). Staining of the same skin sections with a melanocyte-specific marker suggests that the TRPML3-positive cells were melanocytes (Fig. 1*G*). We confirmed the expression of TRPML3 in the mouse melanocyte cell line, melan-a2. A ≈59-kDa band corresponding to the predicted size of mouse TRPML3 was detected by Western blotting in immunoprecipitates from melan-a2 cell lysates (Fig. 1*H*; see controls in SI Fig. 6).

The *Va* mutation is located in the putative S4–S5 linker (Fig. 2*A*), corresponding to a similar region in the well studied K_v channels that links movement of the S1–S4 voltage-sensor/ligand domain to a hydrophobic pocket in the S6 gate of the S5–S6 ion conducting pore (12). Alanine substitution by proline (A863P) in an analogous region of $hNa_V1.7$ produces neuronal hyperexcitability and neuropathy (13). We compared WT, *Va*, and *VaJ* TRPML3 in heterologously expressing HEK293T cells. For WT TRPML3 (Fig. 2*B*), only small nonselective currents were measured (-70 ± 14 pA/pF at -80 mV, $n = 82$) (Fig. 2*G*). Much larger inwardly rectifying currents were seen in TRPML3^{Va}-transfected cells (Fig. 2*B*); TRPML3^{Va}-mediated ($I_{TRPML3\text{-}Va}$) was -456 ± 40 pA/pF (-80 mV; $n = 17$), ≈6-fold larger than

PHYSIOLOGY

Author contributions: H.X., M.D., and L.L. contributed equally to this work; H.X. and M.D. designed research; H.X., M.D., L.L., and X.D. performed research; M.D. contributed new reagents/analytic tools; H.X., M.D., L.L., and X.D. analyzed data; and H.X., M.D., L.L., and D.E.C. wrote the paper.

The authors declare no conflict of interest.

Freely available online through the PNAS open access option.

Abbreviations: $[Ca^{2+}]$, Ca^{2+} concentration; $[X]_i$, intracellular concentration of an ion X; $[X]_o$, extracellular concentration of an ion X; DVF, divalent-free; I–V, current–voltage; KK, lysine lysine; P*n*, postnatal day *n*; S*n*, segment *n*.

†Present address: Department of Molecular, Cellular, and Developmental Biology, University of Michigan, 3089 National Science Building (Krause), 830 North University, Ann Arbor, MI 48105.

‡To whom correspondence should be addressed. E-mail: dclapham@enders.tch.harvard.edu.

This article contains supporting information online at www.pnas.org/cgi/content/full/0709096104/DC1.

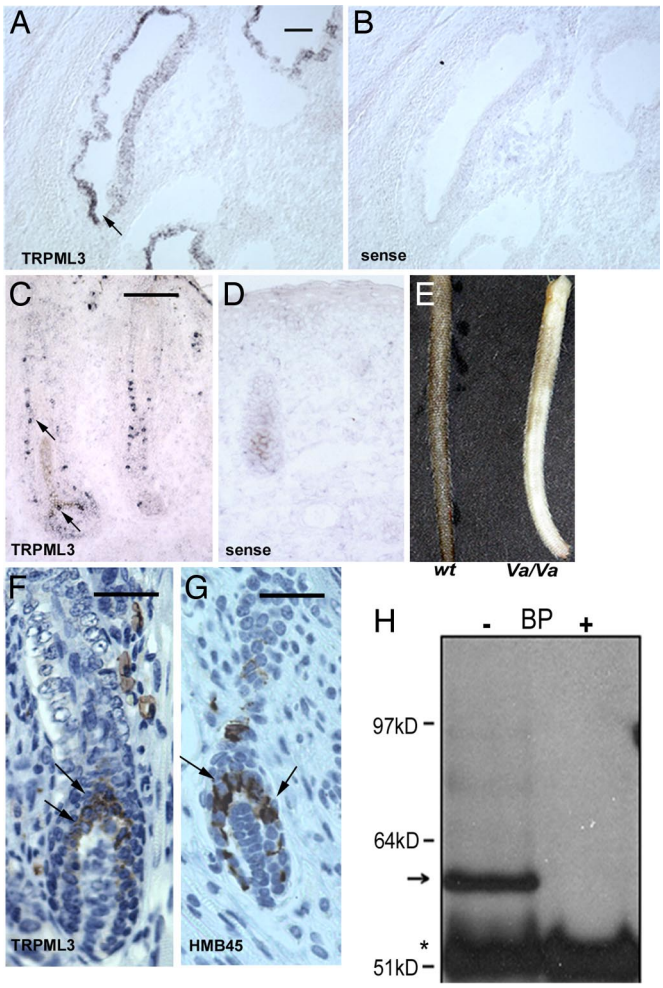

Fig. 1. TRPML3 is highly expressed in the cochlea and melanocytes in skin hair follicles. (*A–D*) *In situ* hybridization of mTRPML3 in P0 mice. (*B* and *D*) Sense probe. (*A*) TRPML3 in the stria vascularis of the cochlea. (Scale bar, 100 μm.) (*C*) TRPML3 expression in a whisker hair follicle. Note the individual cells stained by the antisense probe. (Scale bar, 100 μm.) (*E*) Skin color differences in WT and *Va*/*Va* 6-week-old littermates. (*F* and *G*) Immunohistochemical staining with TRPML3-specific antibodies (*F*) and melanocyte-specific antibodies (HMB45) (*G*) on paraffin-embedded skin sections of P4 WT mice; antibody staining is brown, and the nuclei are blue. TRPML3-specific staining is visible in the cytoplasm of cells in the upper region and sides of the hair bulb (arrows). (Scale bar, 50 μm.) (*G*) Melanocytes in similar locations in the hair bulb. (Scale bar, 50 μm.) (*H*) Immunoprecipitation using anti-TRPML3 antibody was performed in the absence or presence of blocking peptide (BP) from lysates of melan-a2 cells. The TRPML3 band is ≈59 kDa (arrow). The asterisk indicates ab heavy chains; molecular mass markers are shown to the left.

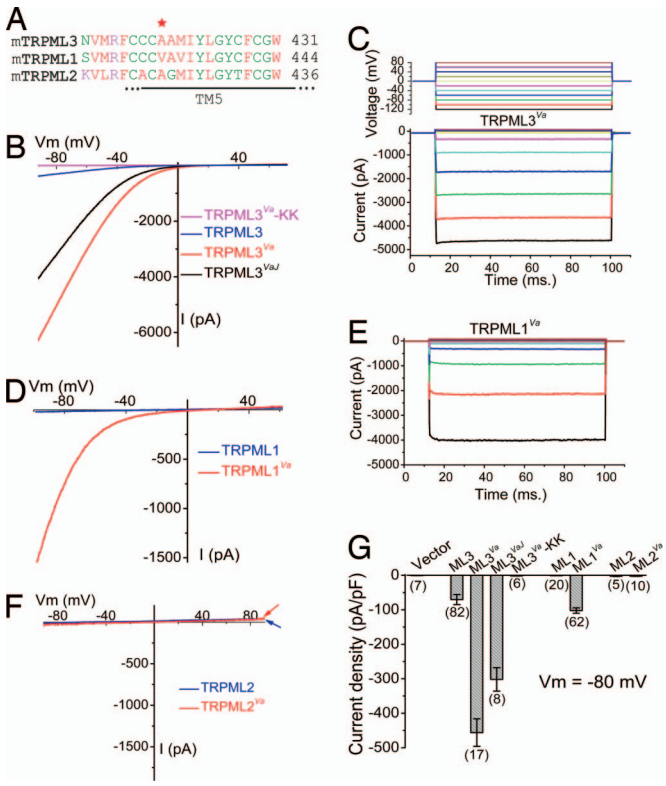

Fig. 2. Large constitutively active inwardly rectifying currents in expressed TRPML1 and TRPML3 *Va* mutants. (*A*) Alignment of TRPML (TRPML1, TRPML2, and TRPML3) protein sequences near the *Va* locus. The red asterisk indicates Ala-419 in TRPML3, which is a proline in *Va* mice. TM5, putative transmembrane S5. (*B*) Representative whole-cell currents in HEK293T cells transfected with WT TRPML3, TRPML3^{Va}, TRPLM3^{VaJ}, and TRPML3^{Va}–KK constructs. Currents were elicited by voltage ramps (−100 to +100 mV, 400 ms) with a 4-s interval between ramps in standard extracellular solution (see *Materials and Methods*). Holding potential (HP) = 0 mV. (*C*) Large inwardly rectifying whole-cell current elicited by voltage steps (−120 mV to +80 mV, 20 mV increments, step duration = 90 ms) in TRPML3^{Va}-expressing cells. HP = 0 mV. $I_{TRPML3\text{-}Va}$ is instantaneously activated at negative potentials. (*D*) Representative whole-cell currents in TRPML1- and TRPML1^{Va}-expressing HEK293T cells. (*E*) $I_{TRPML1\text{-}Va}$ elicited by voltage steps. (*F*) No significant current was measured in HEK293T cells transfected with TRPML2 or TRPML2^{Va}. (*G*) Average inward current densities of TRPML channels at −80 mV normalized by cell capacitance (pF). (*n*) = number of cells.

I_{TRPML3}. Similar results were obtained in transfected melanoma B16 cells (data not shown). The double mutant, $I_{TRPML3\text{-}VaJ}$, was ≈4-fold larger than I_{TRPML3}. The current–voltage relationship (*I–V*) and reversal potentials were similar for all three TRPML3 proteins, suggesting that the *Va* mutation increased channel activity without altering its pore properties. Replacement of two negatively charged acidic amino acids (D458 and D459) by basic amino acids (KK) in the putative pore region of TRPML3 completely eliminated the inwardly rectifying current of both TRPML3 and TRPML3^{Va} (TRPML3-KK, TRPML3^{Va}-KK, Fig. 2 *B* and *G*), suggesting that the overall architecture of TRPML is similar to other TRP (and K_V) channels. TRPML3^{Va}-expressing cells also displayed a strong inwardly rectifying current in response to voltage steps (Fig. 2*C*). $I_{TRPML3\text{-}Va}$ did not inactivate significantly with changes in voltage or time. In addition, $I_{TRPML3\text{-}Va}$ exhibited no cumulative slow inactivation upon repeated depolarization. Thus, TRPML3^{Va}is constitutively active at resting membrane potentials.

Va mutations were made in the homologous positions of TRPML1 and TRPML2. I_{TRPML1} was 1.2 ± 0.2 pA/pF (−80 mV, n = 20, Fig. 2 *D* and *G*), and not significantly different from the current density of vector-transfected HEK293T cells (0.9 ± 0.1 pA/pF, n = 9). In contrast, $I_{TRPML1\text{-}Va}$ was ≈80 times larger (−102 ± 8 pA/pF; n = 62). In the voltage step protocol (Fig. 2*C*), $I_{TRPML1\text{-}Va}$ inwardly rectified with little time dependence at negative potentials (Fig. 2*E*), although $I_{TRPML3\text{-}Va}$ rectification was less steep than for $I_{TRPML1\text{-}Va}$. No significant currents were detected in cells transfected with TRPML2 or TRPML2^{Va} (Fig. 2 *F* and *G*).

Replacement of bath cations by *N*-methyl-D-glucamine ($NMDG^+$) (pH 7.4) suggests that TRPML3^{Va} is a cation-selective ion channel (Fig. 3 *A* and *B*). In isotonic (105 mM) Mg^{2+} or Ca^{2+}, a smaller, less-rectifying current reversed at very positive potentials (> +60 mV) (Fig. 3 *A* and *B*). Inwardly rectifying currents were also measured with monovalent cations

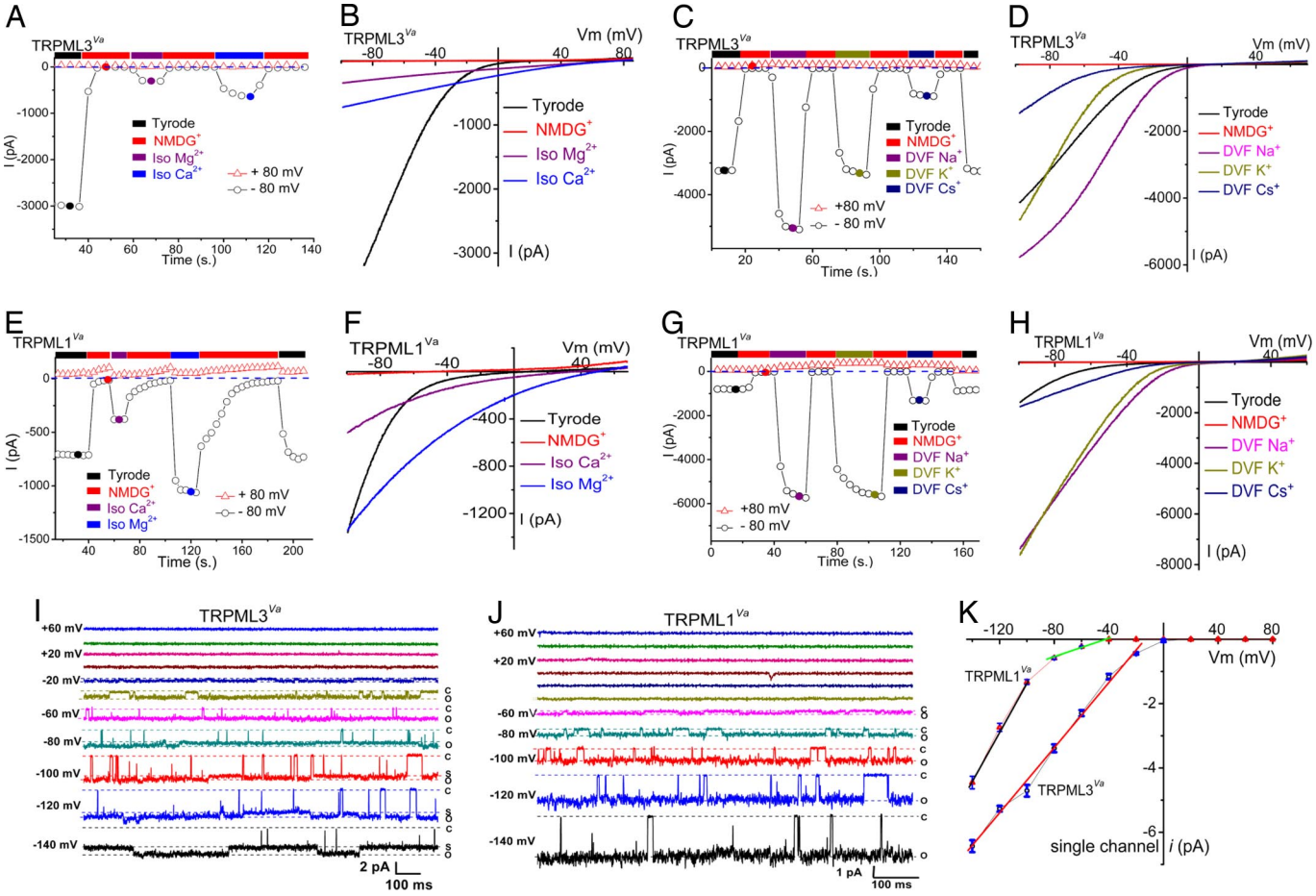

Fig. 3. Permeation properties of TRPML1 and TRPML3 channels. (*A*) TRPML3^{Va} is permeable to both Ca^{2+} and Mg^{2+}. Currents were initially recorded in external solution and elicited by repeated voltage ramps (−100 to +100 mV, 400 ms) with a 4-s interval between ramps. Data at −80 mV and +80 mV were plotted against time. No significant inward current was seen in the $NMDG^+$ (Na^+-free, Ca^{2+}-free) solution. Switching the bath to isotonic (105 mM) Mg^{2+} or Ca^{2+} solution yielded smaller, but measurable, current. Divalent $I_{TRPML3\text{-}Va}$ currents did not inactivate after repetitive voltage ramps. (*B*) Whole-cell *I–V* relations in the presence of isotonic $[Ca^{2+}]_o$ and $[Mg^{2+}]_o$. Note the positive reversal potentials (more than +60 mV). (*C*) Monovalent permeability of $I_{TRPML3\text{-}Va}$ in divalent-free (DVF, $[Ca^{2+}]_i <$ 10 nM) solution. Large inwardly rectifying currents were elicited by DVF, Na^+-containing and DVF, K^+-containing solutions and were smaller in DVF Cs^+ solution. (*D*) Representative *I–V* relations of monovalent Na^+, K^+, and Cs^+ currents in DVF conditions. (*E* and *F*) $I_{TRPML1\text{-}Va}$ Ca^{2+} and Mg^{2+} permeability. Currents elicited by isotonic divalent solutions exhibit weaker voltage dependence than $I_{TRPML1\text{-}Va}$ in external solution. Divalent $I_{TRPML1\text{-}Va}$ currents did not inactivate over longer durations. (*G* and *H*) Large inwardly rectifying monovalent $I_{TRPML1\text{-}Va}$ in DVF conditions. At − 80 mV, Na^+ $I_{TRPML1\text{-}Va}$ in DVF solution was >9-fold larger than the current in external solution. (*I*) Single-channel currents in an inside-out patch excised from a TRPML3^{Va}-expressing HEK293T cell. Pipette contained external solution; the bath was Cs^+-based internal solution (147 mM Cs-Mes). A voltage step [−140 mV to + 80 mV; holding potential (HP) = 0 mV] applied to the inside-out patch elicited channel openings at negative potentials. C and O are closed and open levels, respectively. At negative potentials, substates (S) were frequently observed. (*J*) Single-channel TRPML1^{Va} currents. (*K*) TRPML3^{Va} single-channel conductance (−140 mV to −20 mV) was 49 ± 1 pS (n = 4). TRPML1^{Va} single-channel conductance was 76 ± 4 (−140 mV to −100 mV; n = 5) and 11 ± 0.4 pS (−80 mV to −40 mV; n = 5).

in the absence of divalent cations [divalent-free (DVF); <10 nM] (Fig. 3 *C* and *D*). Cation substitution experiments showed that relative monovalent conductances were $Na^+ > K^+ > Cs^+$. Similar results were also obtained with WT TRPML3 (data not shown). Thus, we conclude that TRPML3/TRPML3^{Va} is a nonselective cationic channel with permeability to Na^+, K^+, Ca^{2+}, and Mg^{2+}. In TRPML1^{Va}-expressing cells, large inwardly rectifying currents were measured in isotonic Ca^{2+} and isotonic Mg^{2+} (Fig. 3 *E* and *F*); in contrast to TRPML3^{Va}, Mg^{2+} currents were larger than Ca^{2+}-mediated currents. Relative monovalent conductances for TRPML1^{Va} were: $Na^+ \approx K^+ > Cs^+$ (Fig. 3 *G* and *H*).

Single-channel properties of TRPML channels were measured in inside-out patch recordings. Similar to whole-cell currents, TRPML3^{Va} and TRPML1^{Va}-mediated single-channel currents were inwardly rectifying (Fig. 3 *I–K* and SI Fig. 7). Channel openings with large amplitudes were recorded at negative potentials, whereas no openings were resolved at positive potentials. At very negative potentials (less than −80 mV), both TRPML1^{Va} and TRPML3^{Va} channels were usually open ($P_{open} >$ 0.7). For TRPML3^{Va}, the mean open and closed times at −120 mV were 282 ± 116 and 2.1 ± 0.9 ms, respectively. For TRPML1^{Va}, the mean open and closed times at −120 mV were 113 ± 41 and 6.1 ± 2.6 ms, respectively. The single-channel conductance for TRPML3^{Va} (−140 mV to −20 mV) was 49 ± 1 pS. Single-channel TRPML1^{Va} conductances were 76 ± 4 pS (−140 mV to −100 mV), and 11 ± 0.4 pS (−80 mV to −40 mV), respectively.

TRPML channels are believed to be primarily targeted to endosomes or lysosomes (3, 14). A salient feature of acidified endosomes and lysosomes is low-intravesicular pH. Also, previous reports suggested that TRPML1 was permeant to protons (9). We measured TRPML channels at low extracellular pH (analogous to the luminal pH exposure of the channel's intravesicular surface). Because protons also activated an endogenous Cl^- conductance that was strongly outwardly rectifying

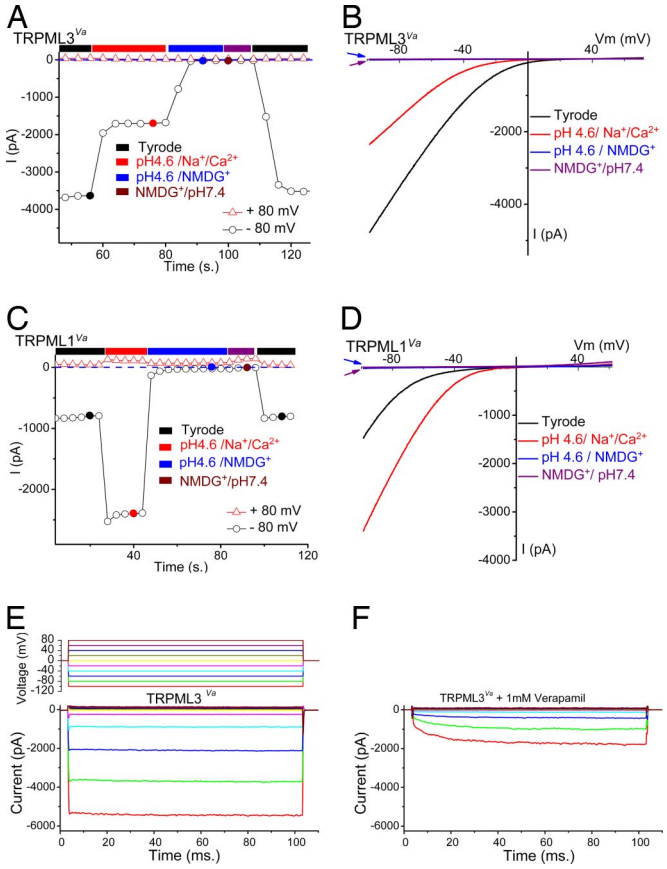

Fig. 4. TRPML1 and TRPML3 pH dependence and pharmacological block. (*A* and *B*) TRPML3^{Va} is a proton-impermeant cation channel inhibited by low extracellular pH. (*A*) $I_{TRPML3\text{-}Va}$ in external solution was inhibited by ≈60% when the pH of the bath solution was decreased to 4.6. Replacement of permeable cations ($Na^+/Ca^{2+}/Mg^{2+}/K^+$) by $NMDG^+$ at pH 4.6 eliminated most inward current. (*B*) Representative currents in external, pH 4.6, low-pH $NMDG^+$, and pH 7.4 $NMDG^+$ solutions. The amplitudes of $NMDG^+$ currents at pH 7.4 (blue arrow) and pH 4.6 (red arrow) are similar. (*C* and *D*) TRPML1^{Va} is a proton-impermeant cation channel strongly enhanced by low extracellular pH. (*C*) $I_{TRPML1\text{-}Va}$ in external solution increased ≈3-fold by acidification to pH 4.6. No significant inward current was seen in $NMDG^+$ solutions (pH 7.4 and pH 4.6). (*D*) Representative whole-cell currents in pH 4.6 external, low-pH $NMDG^+$, and pH 7.4 $NMDG^+$ solutions. Note that the $NMDG^+$-elicited currents at pH 7.4 (blue arrow) and pH 4.6 (red arrow) are almost indistinguishable. (*E*) Large inwardly rectifying whole-cell current in a TRPML3^{Va}-expressing cell (protocol, *Top*) in external solution. (*F*) Verapamil (1 mM) inhibits and slows activation of currents at negative potentials.

(15), gluconate$^-$ or Mes$^-$ was usually used to replace most of the Cl^- ($[\text{remaining } Cl^-]_o$ = 5–10 mM) for all low-pH bath solutions. In the presence of permeable cations (low-pH "Tyrode's solution"), pH 4.6 inhibited $I_{TRPML3\text{-}Va}$ by 67 ± 2% (n = 7) (Fig. 4 *A* and *B*). No significant inward current was measured when $NMDG^+$ replaced all cations in the bath solution at pH 4.6, suggesting that TRPML3 was not significantly permeant to protons. In contrast to $I_{TRPML3\text{-}Va}$, $I_{TRPML1\text{-}Va}$ was potentiated by acid (pH 4.6) (Fig. 4 *C* and *D*) by 2.9 ± 0.2-fold (n = 5), but again no significant current was observed when $NMDG^+$ replaced all of the cations in the low-pH bath solution (Fig. 4 *C* and *D*). A small inward current (<30 pA) was observed in both TRPML-transfected and nontransfected control cells (SI Fig. 8). Thus, TRPML1 is a proton-impermeant, nonselective cation channel modulated by pH. These results are also in disagreement with a previous report on a current probably misidentified as TRPML1 in which an outwardly rectifying current was inhibited by acid (16).

TRP pharmacology is still in its infancy, and few specific blockers have been identified. TRPML1 and TRPML3 were not inhibited by 2APB (200 μM), SKF 96365 (50 μM), amiloride (100 μM), ruthenium red (10 μM), or nifedipine (100 μM). However, at high concentrations of verapamil (1 mM), TRPML3 activation was slowed 10-fold from τ = 0.1 ± 0.01 ms (n = 4, −100 mV) to τ = 1 ± 0.1 ms (n = 4; Fig. 4 *E* and *F*). Similar effects were observed for $I_{TRPML1\text{-}Va}$.

TRPML3 is natively expressed in melan-a2 cells (see Fig. 1*H*). To determine whether TRPML3 mutants differed in their trafficking or localization, we transfected melan-a2 cells with N-terminal GFP-tagged TRPML3 (Fig. 5*A*), TRPML3^{Va} (Fig. 5*B*), and TRPML3^{Va}-KK (Fig. 5*C*). TRPML3 was present in widespread vesicular compartments (Fig. 5*A*), whereas TRPML3^{Va} appeared to be partially mislocalized within the cell (Fig. 5*B*). More strikingly, most of the TRPML3^{Va}-transfected cells rounded up (80 ± 9%) and were stained by the Ethidium bromide homodimer EthD-1 (71 ± 22%), suggesting a loss of membrane integrity (Fig. 5*G* and SI Fig. 6). The frequency of round cells and EthD-1-positive cells was significantly less in TRPML3-transfected cells (19 ± 3% and 5 ± 7%, respectively (Fig. 5*G* and SI Fig. 6), suggesting that the constitutive activity of TRPML3^{Va} was toxic.

To determine whether cell toxicity resulted from channel-mediated cation influx, melan-a2 cells were transfected with the nonfunctional TRPML3^{Va}-KK pore mutant (Fig. 5*C*). Although also mislocalized compared with the WT expression (Fig. 5 *C* vs. *A*), the number of dying cells was significantly reduced when compared with the TRPML3^{Va}-expressing cells (Fig. 5*G*). The toxicity of constitutively active TRPML3 could result from sustained cation influx across the plasma membrane or from equilibration of cations across the late endosomal/lysosomal membranes. TRPML3 and TRPML3^{Va}-KK transfected melan-a2 cell resting $[Ca^{2+}]$ levels were similar to nontransfected cells (Fig. 5 *D* and *E*), whereas TRPML3^{Va}-expressing cells showed significantly higher $[Ca^{2+}]_i$ (Fig. 5*F*). Removal of extracellular Ca^{2+} reduced $[Ca^{2+}]_i$ in TRPML3^{Va}-expressing cells, but not in TRPML3 and TRPML3^{Va}-KK-transfected cells. We conclude that the constitutive activity of expressed plasma membrane TRPML3^{Va} induced Ca^{2+} overload and cell death (Fig. 5*H*).

Skin sections from WT or *Va* homozygous littermates were stained with TRPML3 antibody or tyrosinase to label melanocytes (10). In WT skin sections, 26% of hair follicles contained melanocytes (Fig. 5 *I* and *J*). The presence of TRPML3-expressing cells in the hair bulb was further confirmed by *in situ* hybridization (Fig. 5*K*). In contrast, no melanocytes were detected in the hair follicles of skin sections derived from the homozygous *Va* mouse (Fig. 5 *L* and *M*), nor was the hair bulb labeled by the TRPML3-specific *in situ* probe (Fig. 5*N*). We conclude most melanocytes are lost from hair follicles of the 6-week-old *Va* mice, resulting in lighter fur and skin color (Fig. 1*E*).

Discussion

The primarily intracellular localization of TRPML ion channels had prevented the direct study of mucolipin currents. The varitint–waddler mouse, identified >60 years ago, provides a fortuitous window into the workings of the TRPML family. Based on past work, mutations in the S4/S5 linker junction alter channel gating (17). Analogous mutations in TRPML1 and TRPML3 result in large conductances across the plasma membrane, even at resting membrane potentials. TRPML1 and TRPML3, like most TRP ion channels, are cation-nonselective and Ca^{2+}-permeant; no H^+ conductance was detected in this study. Constitutive activity on the plasma membrane is a deleterious gain-of-function, killing melanocytes over time and thus reducing hair and skin pigmentation. These results agree with of the observed loss of melanocytes in the cochlea of *Va*/*Va* mice (18). It is likely that cell loss due to mutant TRPML3 in the

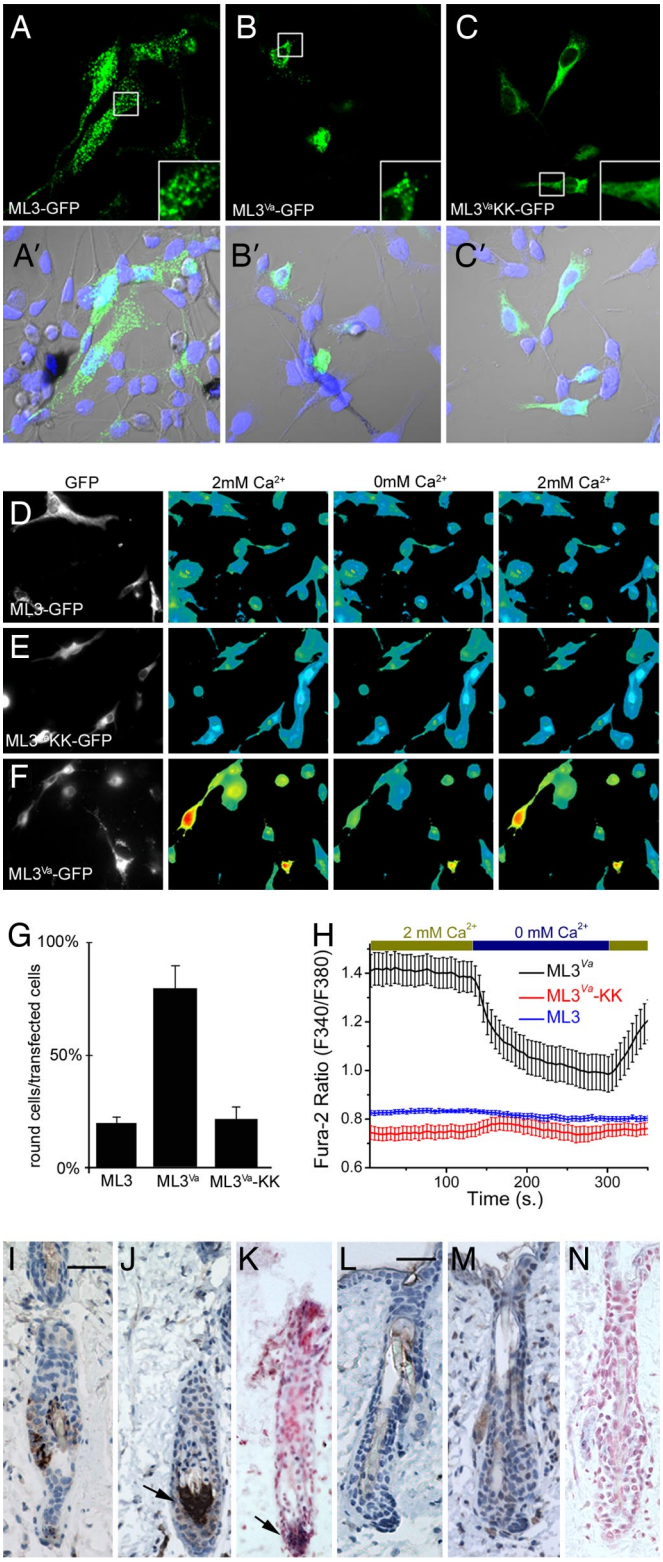

Fig. 5. Elevated $[Ca^{2+}]_i$ in TRPML3^{Va}-expressing cells and melanocyte cell death. (*A–C*) Melan-a2 cells were transfected with GFP-tagged TRPML3 (*A* and *A′*), TRPML3^{Va} (*B* and *B′*), and TRPML3^{Va}-KK (*C* and *C′*) constructs and assayed after 48 h. Note punctate distribution of TRPML3 in melan-a2 cells (*A Inset*). (*B*) Round morphology of TRPML3^{Va}-expressing cells. (*C* and *C Inset*) Cells expressing the TRPML3^{Va}-KK mutant attach and spread; the fluorescence signal is not punctate. (*A′–C′*) Cells were stained with TO-PRO3 nuclear stain. (*D–F*) Melan-a2 cells were transfected with GFP-tagged TRPML3 (*D*), TRPML3^{Va}-KK (*E*), and TRPML3^{Va} (*F*) constructs; $[Ca^{2+}]_i$ was measured after 20 h. Resting $[Ca^{2+}]_i$ in TRPML3- and TRPML3^{Va}-KK-transfected cells was similar to nontransfected cells. In contrast, $[Ca^{2+}]_i$ was significantly elevated in TRPML3^{Va}-transfected cells in 2 mM extracellular $[Ca^{2+}]$. Representative data are from four to eight experiments. (*G*) Quantification of round vs. spread cells after transfection with the indicated construct (80 ± 9% round cells for TRPML3^{Va} vs. 19 ± 3% round cells for WT TRPML3). The levels of KK mutant were similar to those of WT (19 ± 3% round cells for TRPML3 vs. 22 ± 6% round cells for TRPML3^{Va}-KK transfected cells; $n = 3$ experiments). (*H*) In TRPML3^{Va}-transfected cells, Fura-2 ratios in 2 mM $[Ca^{2+}]_o$ (1.4 ± 0.06) drop when $[Ca^{2+}]_o$ is reduced (nominal 0 mM Ca^{2+}, 1 mM EGTA; 0.99 ± 0.07). $[Ca^{2+}]_i$ did not change significantly after removal of extracellular Ca^{2+} for TRPML3 and TRPML3^{Va}-KK transfected cells (0.82 + 0.01 and 0.75 + 0.03). (*I*, *J*, *L*, and *M*). Representative immunohistochemical staining, using tyrosinase- (*I* and *L*) and TRPML3- (*J* and *M*) specific antibodies of paraffin-embedded skin sections from 6-week-old WT (*I–K*) and *Va*/*Va* (*L–N*) mice. (*K* and *N*) Sections were also stained for TRPML3 by *in situ* hybridization. Antibody staining is brown; nuclei are stained blue. The *in situ* signal is visible as a blue precipitate with nuclei stained in red. (Scale bar, 50 μm.) (*I*) Tyrosinase staining of WT hair follicles indicates that melanocytes are primarily in the bulb of the hair follicle. (*J*) Staining with a TRPML3-specific antibody indicates that TRPML3-positive cells are localized to a similar region in adult mouse hair follicle. (*K*) TRPML3-specific *in situ* hybridization; TRPML3 antibody and the *in situ* probe stain similar regions in the hair follicle bulb. (*L* and *M*) Immunohistochemical staining, using tyrosinase- and TRPML3-specific antibodies, was performed side by side with the WT slides. Neither tyrosinase- nor TRPML3- specific signal was detected in the hair bulb of *Va*/*Va* mice. In the WT skin sections, ≈26% of the hair follicles were labeled by the tyrosinase antibody (90/347) or by the TRPML3 specific antibody (66/255). No tyrosinase- or TRPML3-specific staining was detected in *Va*/*Va* mouse hair follicle bulbs (≈300 hair follicles were analyzed). (*N*) TRPML3 is absent in hair follicle bulbs from *Va*/*Va* skin sections (*in situ* hybridizations).

cochlea and vestibular apparatus underlies the deafness and the circling behavior of *Va*/*Va* mice. The low viability of *Va*/*Va* mice will require further study. A more important question left unanswered is whether the primary function of TRPML3 is endosomal/lysosomal, on the plasma membrane, or both. Interestingly, several TRP ion channels appear to function on both intracellular membranes and the plasma membrane, and rapid translocation can occur in response to signaling molecules (19).

Materials and Methods

Molecular Biology. Full-length mouse TRPML1, TRPML2, and TRPML3 were cloned from a mouse macrophage cDNA library and cloned into the EGFP-C2 vector (Clontech) or pcDNA3 containing an HA tag at the 5′end.

Antibodies and Immunoprecipitation. Rabbit polyclonal antibodies (Chemicon) were raised against N-terminal (amino acids 5–20) and C-terminal (amino acids 528–547) peptides of TRPML3 and affinity-purified (Pierce). TRPML3 antibodies did not recognize overexpressed TRPML1 or TRPML2. Goat anti-tyrosinase antibody was from Santa Cruz Biotechnologies, and mouse HMB45 was from Dako.

HA-TRPML3-transfected cells or melan-a2 cells were solubilized in lysis buffer (50 mM Tris·Cl, pH 8.0/150 mM NaCl/1% Triton X-100) supplemented with protease inhibitor mixture (Roche) and immunoprecipitated with TRPML3 CT antibody.

Immunocytochemistry and Confocal Microscopy. Cells were fixed with 4% formaldehyde, permeabilized with 0.2% Triton X-100, and blocked by 10% goat serum in PBS. Cells were labeled with TRPML3 antibodies and Cy5-conjugated goat anti-rabbit IgG (Invitrogen) or TO-PRO3 (Invitrogen). Confocal images were obtained with a 60 × 1.4 N.A. objective, zoom 1 (Olympus Fluoview 1000).

Transfection. Melan-a2 cells were transfected by using electroporation (Amaxa) and assayed 20–48 h after transfection.

HEK293T cells and B16 cells were transfected by using Lipofectamine (Invitrogen) and assayed 24 h after transfection.

In situ hybridization was performed by using a 650-bp fragment from the 3′ UTR of mouse TRPML3 cloned into the pCR4-Topo vector. Automated ISH was performed on paraffin-embedded sections (Discovery System; Ventana Medical Systems). Detection was performed by biotinylated anti-digoxigenin antibody (Biogenex) followed by streptavidin-alkaline-phosphatase conjugate and visualized by nitroblue tetrazolium/5-bromo-4-chloro-3-indolyl phosphate substrate reaction (Ventana BlueMap detection kit). Slides were counterstained by nuclear fast red (Vector Laboratories). Frozen section staining was performed as described in ref. 20.

Mice. C57BL/6 and heterozygous Mcoln^{Va} (TRPML3^{Va}) were obtained from The Jackson Laboratory. The breeding scheme for the Mcoln^{Va} line was +/+ × Va/+ or Va/+ × Va/+, and mice were genotyped as described in ref. 5.

Immunohistochemistry. Formalin-fixed paraffin-embedded tissue sections (5μ) were pretreated with 10 mM citrate, pH 6.0 (Zymed; decloaking chamber, BioCare Medical). Slides were pretreated with peroxidase block (Dako) for 5 min. Primary antibodies were diluted 1:250 (ML3NT) and 1:100 (tyrosinase and HMB45). Slides were washed, and anti-rabbit horseradish peroxidase-conjugated antibody (Envision detection kit, Dako) was applied. Immunoperoxidase staining was developed by using a DAB chromagen kit (Dako) and counterstained with hematoxylin.

Electrophysiology. Recordings were performed in transiently transfected HEK293T cells. No significant functional difference was observed between EGFP-tagged and HA-tagged TRPML^{Va} constructs. Transfected cells, cultured at 37°C, were plated onto glass coverslips and recorded 24 h after transfection. Unless otherwise stated, the pipette solution contained 147 mM Cs, 120 mM methane-sulfonate, 8 mM NaCl, 10 mM EGTA, 2 mM Mg-ATP, and 20 mM Hepes (pH 7.2; free $[Ca^{2+}]_i < 10$ nM). Standard extracellular bath Tyrode's solution contained 153 mM NaCl, 5 mM KCl, 2 mM $CaCl_2$, 1 mM $MgCl_2$, 20 mM Hepes, and 10 mM glucose (pH 7.4). Low-pH external solution contained 150 mM Na-gluconate, 5 mM KCl, 2 mM $CaCl_2$, 1 mM $MgCl_2$,10 mM Hepes, and 10 mM Mes (pH 4.6). $NMDG^+$ solution contained 160 mM NMDG·Cl, 20 mM Hepes, and 10 mM glucose (pH 7.4). Low-pH $NMDG^+$ solution contained 150 mM NMDG, 10 mM glucose, 10 mM Mes, 10 Hepes (pH adjusted to 4.6, using methanesulfonic acid). DVF monovalent solutions contained 30 mM glucose, 20 mM Hepes, 10 mM EDTA, 160 mM KCl, NaCl, or CsCl (pH 7.4; free $Ca^{2+} < 10$ nM). Data were collected by using an Axopatch 2A and Digidata 1440 and pClamp software, Version 10.0 (Axon Instruments). Whole-cell currents and single-channel recordings were digitized at 10 kHz and filtered at 2 kHz. Capacity current was nulled; series resistance compensation was 60–85%. All experiments were conducted at room temperature (≈21–23°C). All recordings were analyzed with pCLAMP10 (Axon Instruments) and Origin software, Version 7.5 (OriginLab).

Ca^{2+} Imaging. Twenty hours after transfection, melan-a2 cells were loaded with 5 μM Fura-2AM and 0.02% pluronic acid at 37°C for 60 min, then washed for 10–30 min. GFP fluorescence was monitored at 440 nm (F440). Fura-2 ratios (F340/F380) were determined $[Ca^{2+}]_i$, and experiments were repeated four to eight times; representative traces are shown in figures.

Reagents. 2APB, verapamil, nifedipine, amiloride, and SKF96365 were prepared in stock solution containing dimethylsulfulfonate (DMSO; < 0.1% final).

Data Analysis. Group data are presented as mean ± SEM. Statistical comparisons were made with analysis of variance and the ANOVA test. $P < 0.05$ was considered statistically significant.

We thank the core facility of the Brigham and Women's Hospital for help with the immunohistochemistry and *in situ* hybridization, Dr. Urs Berger for assistance, Dr. Bimal Desai for his stimulating discussion throughout the project, and members of the Clapham and Xu laboratories for discussion and helpful comments. H.X. was supported by the startup funds from the Department of MCDB and Biological Science Scholar Program, the University of Michigan.

1. Pryor PR, Reimann F, Gribble FM, Luzio JP (2006) *Traffic* 7:1388–1398.
2. Venkatachalam K, Hofmann T, Montell C (2006) *J Biol Chem* 281:17517–17527.
3. Vergarajauregui S, Puertollano R (2006) *Traffic* 7:337–353.
4. Song Y, Dayalu R, Matthews SA, Scharenberg AM (2006) *Eur J Cell Biol* 85:1253–1264.
5. Di Palma F, Belyantseva IA, Kim HJ, Vogt TF, Kachar B, Noben-Trauth K (2002) *Proc Natl Acad Sci USA* 99:14994–14999.
6. Cloudman AM, Bunker LE (1945) *J Hered* 36:258–263.
7. Lane PW (1972) *J Hered* 63:135–140.
8. Kiselyov K, Chen J, Rbaibi Y, Oberdick D, Tjon-Kon-Sang S, Shcheynikov N, Muallem S, Soyombo A (2005) *J Biol Chem* 280:43218–43223.
9. Soyombo AA, Tjon-Kon-Sang S, Rbaibi Y, Bashllari E, Bisceglia J, Muallem S, Kiselyov K (2006) *J Biol Chem* 281:7294–7301.
10. Botchkareva NV, Botchkarev VA, Gilchrest BA (2003) *J Investig Dermatol Symp Proc* 8:76–79.
11. Nishimura EK, Granter SR, Fisher DE (2005) *Science* 307:720–724.
12. Long SB, Campbell EB, MacKinnon R (2005) *Science* 309:897–903.
13. Harty TP, Dib-Hajj SD, Tyrrell L, Blackman R, Hisama FM, Rose JB, Waxman SG (2006) *J Neurosci* 26:12566–12575.
14. Zeevi DA, Frumkin A, Bach G (2007) *Biochim Biophys Acta* 1772:851–858.
15. Xu H, Jin J, DeFelice LJ, Andrews NC, Clapham DE (2004) *PLoS Biol* 2:E50.
16. Raychowdhury MK, Gonzalez-Perrett S, Montalbetti N, Timpanaro GA, Chasan B, Goldmann WH, Stahl S, Cooney A, Goldin E, Cantiello HF (2004) *Hum Mol Genet* 13:617–627.
17. Clapham DE (2003) *Nature* 426:517–524.
18. Cable J, Steel KP (1998) *Hear Res* 123:125–136.
19. Ramsey IS, Delling M, Clapham DE (2006) *Annu Rev Physiol* 68:619–647.
20. Xu H, Delling M, Jun JC, Clapham DE (2006) *Nat Neurosci* 9:628–635.